9

Fast BEM Based Methods for Heat Transfer Simulation

Jure Ravnik and Leopold Škerget
University of Maribor, Faculty of Mechanical Engineering
Slovenia

1. Introduction

Development of numerical techniques for simulation of fluid flow and heat transfer has a long standing tradition. Computational fluid dynamics has evolved to a point where new methods are needed only for special cases. In this chapter we introduce a Fast Boundary Element Method (BEM), which enables accurate prediction of vorticity fields. Vorticity field is defined as a curl of the velocity field and is an important quantity in wall bounded flows. Vorticity is generated on the walls and diffused and advected into the flow field. Using BEM, we are able to accurately predict boundary values of vorticity as a part of the nonlinear system of equations, without the use of finite difference approximations of derivatives of the velocity field. The generation of vorticity on the walls is important for the development of the flow field, shear strain, shear velocity and heat transfer.

The developed method will be used to simulate natural convection of pure fluids and nanofluids. Over the last few decades buoyancy driven flows have been widely investigated. Cavities under different inclination angles with respect to gravity, heated either differentially on two opposite sides or via a hotstrip in the centre, are usually the target of research. Natural convection is used in many industrial applications, such as cooling of electronic circuitry, nuclear reactor insulation and ventilation of rooms.

Research of the natural convection phenomena started with the two-dimensional approach and has been recently extended to three dimensions. A benchmark solution for two-dimensional flow and heat transfer of an incompressible fluid in a square differentially heated cavity was presented by Davies (1983). Stream function-vorticity formulation was used. Vierendeels et al. (2001; 2004) and Škerget & Samec (2005) simulated compressible fluid in a square differentially heated cavity using multigrid and BEM methods. Rayleigh numbers between $Ra = 10^2$ and $Ra = 10^7$ were considered. Weisman et al. (2001) studied the transition from steady to unsteady flow for compressible fluid in a $1:4$ cavity. They found that the transition occurs at $Ra \approx 2 \times 10^5$. Ingber (2003) used the vorticity formulation to simulate flow in both square and $1:8$ differentially heated cavities. Tric et al. (2000) studied natural convection in a 3D cubic cavity using a pseudo-spectra Chebyshev algorithm based on the projection-diffusion method with spatial resolution supplied by polynomial expansions. Lo et al. (2007) also studied a 3D cubic cavity under five different inclinations $\vartheta = 0^o, 15^o, 30^o, 45^o, 60^o$. They used a differential quadrature method to solve the velocity-vorticity formulation of Navier-Stokes equations employing higher order polynomials to approximate differential operators. Ravnik et al. (2008) used a combination of single domain and sub domain BEM to solve the velocity-vorticity formulation of Navier-Stokes equations for fluid

flow and heat transfer.

Simulations as well as experiments of turbulent flow were also extensively investigated. Hsieh & Lien (2004) considered numerical modelling of buoyancy-driven turbulent flows in cavities using RANS approach. 2D DNS was performed by Xin & Quéré (1995) for an cavity with aspect ratio 4 up to Rayleigh number, based on the cavity height, 10^{10} using expansions in series of Chebyshev polynomials. Ravnik et al. (2006) confirmed these results using a 2D LES model based on combination of BEM and FEM using the classical Smagorinsky model with Van Driest damping. Peng & Davidson (2001) performed a LES study of turbulent buoyant flow in a $1:1$ cavity at $Ra = 1.59 \cdot 10^9$ using a dynamic Smagorinsky model as well as the classical Smagorinsky model with Van Driest damping.

Low thermal conductivity of working fluids such as water, oil or ethylene glycol led to the introduction of nanofluids. Nanofluid is a suspension consisting of uniformly dispersed and suspended nanometre-sized (10–50 nm) particles in base fluid, pioneered by Choi (1995). Nanofluids have very high thermal conductivities at very low nanoparticle concentrations and exhibit considerable enhancement of convection (Yang et al., 2005). Intensive research in the field of nanofluids started only recently. A wide variety of experimental and theoretical investigations have been performed, as well as several nanofluid preparation techniques have been proposed (Wang & Mujumdar, 2007).

Several researchers have been focusing on buoyant flow of nanofluids. Oztop & Abu-Nada (2008) performed a 2D study of natural convection of various nanofluids in partially heated rectangular cavities, reporting that the type of nanofluid is a key factor for heat transfer enhancement. They obtained best results with Cu nanoparticles. The same researchers (Abu-Nada & Oztop, 2009) examined the effects of inclination angle on natural convection in cavities filled with Cu–water nanofluid. They reported that the effect of nanofluid on heat enhancement is more pronounced at low Rayleigh numbers. Hwang et al. (2007) studied natural convection of a water based Al_2O_3 nanofluid in a rectangular cavity heated from below. They investigated convective instability of the flow and heat transfer and reported that the natural convection of a nanofluid becomes more stable when the volume fraction of nanoparticles increases. Ho et al. (2008) studied effects on nanofluid heat transfer due to uncertainties of viscosity and thermal conductivity in a buoyant cavity. They demonstrated that usage of different models for viscosity and thermal conductivity does indeed have a significant impact on heat transfer. Natural convection of nanofluids in an inclined differentially heated square cavity was studied by Ögüt (2009), using polynomial differential quadrature method. Stream function-vorticity formulation was used for simulation of nanofluids in two dimensions by Gümgüm & Tezer-Sezgin (2010).

Forced and mixed convection studies were also performed. Abu-Nada (2008) studied the application of nanofluids for heat transfer enhancement of separated flows encountered in a backward facing step. He found that the high heat transfer inside the recirculation zone depends mainly on thermophysical properties of nanoparticles and that it is independent of Reynolds number. Mirmasoumi & Behzadmehr (2008) numerically studied the effect of nanoparticle mean diameter on mixed convection heat transfer of a nanofluid in a horizontal tube using a two-phase mixture model. They showed that the convective heat transfer could be significantly increased by using particles with smaller mean diameter. Akbarinia & Behzadmehr (2007) numerically studied laminar mixed convection of a nanofluid in horizontal curved tubes. Tiwari & Das (2007) studied heat transfer in a lid-driven differentially heated square cavity. They reported that the relationship between heat transfer and the volume fraction of solid particles in a nanofluid is nonlinear. Torii (2010) experimentally

studied turbulent heat transfer behaviour of nanofluid in a circular tube, heated under constant heat flux. He reported that the relative viscosity of nanofluids increases with concentration of nanoparticles, pressure loss of nanofluids is slightly larger than that of pure fluid and that heat transfer enhancement is affected by occurrence of particle aggregation.

Development of numerical algorithms capable of simulating fluid flow and heat transfer has a long standing tradition. A vast variety of methods was developed and their characteristics were examined. In this work we are presenting an algorithm, which is able to simulate 3D laminar viscous flow coupled with heat transfer by solving the velocity-vorticity formulation of Navier-Stokes equations using fast BEM. The velocity-vorticity formulation is an alternative form of the Navier-Stokes equation, which does not include pressure. The unknown field functions are the velocity and vorticity. In an incompressible flow, both are divergence free. Daube (1992) pointed out that the correct evaluation of boundary vorticity values is essential for conservation of mass. Thus, the main challenge of velocity-vorticity formulation lies in the determination of boundary vorticity values. Several different approaches have been proposed for the determination of vorticity on the boundary. Wong & Baker (2002) used a second-order Taylor series to determine the boundary vorticity values explicitly. Daube (1992) used an influence matrix technique to enforce both the continuity equation and the definition of the vorticity in the treatment of the 2D incompressible Navier-Stokes equations. Liu (2001) recognised that the problem is even more severe when he extended it to three dimensions. Lo et al. (2007) used the differential quadrature method. Sellountos & Sequeira (2008) proposed a hybrid multi BEM scheme in combination with local boundary integral equations and radial basis functions for 2D fluid flow. Škerget et al. (2003) proposed the usage of single domain BEM to obtain a solution of the kinematics equation in tangential form for the unknown boundary vorticity values and used it in 2D. This work was extended into 3D using a linear interpolation in combination with FEM by Žunič et al. (2007) and using quadratic interpolation by Ravnik et al. (2009a) for uncoupled flow problems.

The BEM uses the fundamental solution of the differential operator and the Green's theorem to rewrite a partial differential equation into an equivalent boundary integral equation. After discretization of only the boundary of the problem domain, a fully populated system of equations emerges. The number of degrees of freedom is equal to the number of boundary nodes. This reduction of the dimensionality of the problem is a major advantage over the volume based methods. Fundamental solutions are known for a wide variety of differential operators (Wrobel, 2002), making BEM applicable for solving a wide range of problems.

Unfortunately, integral equations of nonhomogeneous and nonlinear problems, such as heat transfer in fluid flow, include a domain term. In this work, we solve the velocity-vorticity formulation of incompressible Navier-Stokes equations. The formulation joins the Poisson type kinematics equation with diffusion advection type equations of vorticity and heat transport. These equations are nonhomogenous and nonlinear. In order to write discrete systems of linear equations for such equations, matrices of domain integrals must be evaluated. Such domain matrices, since they are full and unsymmetrical, require a lot of storage space and algebraic operations with them require a lot of CPU time. Thus the domain matrices present a bottleneck for any BEM based algorithm effectively limiting the maximal usable mesh size through their cost in storage and CPU time.

The dual reciprocity BEM (Partridge et al. (1992), Jumarhon et al. (1997)) is one of the most popular techniques to eliminate the domain integrals. It uses expansion of the nonhomogenous term in terms of radial basis functions. Several other approaches that enable construction of data sparse approximations of fully populated matrices are also

known. Hackbusch & Nowak (1989) developed a panel clustering method, which also enables approximate matrix vector multiplications with decreased amount of arithmetical work. A class of hierarchical matrices was introduced by Hackbusch (1999) with the aim of reducing the complexity of matrix-vector multiplications. Bebendorf & Rjasanow (2003) developed an algebraic approach for solving integral equations using collocation methods with almost linear complexity. Methods based on the expansion of the integral kernel (Bebendorf, 2000) have been proposed as well. Fata (2010) proposed treatment of domain integrals by rewriting them as a combination of surface integrals whose kernels are line integrals. Ravnik et al. (2004) developed a wavelet compression method and used it for compression of single domain BEM in 2D. Compression of single domain full matrices has also been the subject of research of Eppler & Harbrecht (2005).

The algorithm proposed in this chapter tackles the domain integral problem using two techniques: a kernel expansion method based single domain BEM is employed for fast solution of the kinematics equation and subdomain BEM is used for diffusion-advection type equations.

In the subdomain BEM (Popov et al., 2007), integral equations are written for each subdomain (mesh element) separately. We use continuous quadratic boundary elements for the discretization of function and discontinuous linear boundary element for the discretization of flux. By the use of discontinuous discretization of flux, all flux nodes are within boundary elements where the normal and the flux are unambiguously defined. The corners and edges, where the normal is not well defined, are avoided. The singularities of corners and edges were dealt with special singular shape functions by Ong & Lim (2005) and by the use of additional nodes by Gao & Davies (2000). By the use of a collocation scheme, a single linear equation is written for every function and flux node in every boundary element. By using compatibility conditions between subdomains, we obtain an over-determined system of linear equations, which may be solved in a least squares manner. The governing matrices are sparse and have similar storage requirements as the finite element method. Subdomain BEM was applied on the Laplace equation by Ramšak & Škerget (2007) and on the velocity-vorticity formulation of Navier-Stokes equations by Ravnik et al. (2008; 2009a).

The second part of the algorithm uses fast kernel expansion based single domain BEM. The method is used to provide a sparse approximation of the fully populated BEM domain matrices. The storage requirements of the sparse approximations scale linearly with the number of nodes in the domain, which is a major improvement over the quadratic complexity of the full BEM matrices. The technique eliminates the storage and CPU time problems associated with application of BEM on nonhomogenous partial differential equations.

The origins of the method can be found in a fast multipole algorithm (FMM) for particle simulations developed by Greengard & Rokhlin (1987). The algorithm decreases the amount of work required to evaluate mutual interaction of particles by reducing the complexity of the problem from quadratic to linear. Ever since, the method was used by many authors for a wide variety of problems using different expansion strategies. Recently, Bui et al. (2006) combined FMM with the Fourier transform to study multiple bubbles dynamics. Gumerov & Duraiswami (2006) applied the FMM for the biharmonic equation in three dimensions. The boundary integral Laplace equation was accelerated with FMM by Popov et al. (2003). In contrast to the contribution of this paper, where the subject of study is the application of FMM to obtain a sparse approximation of the domain matrix, the majority of work done by other authors dealt with coupling BEM with FMM for the boundary matrices. Ravnik et al. (2009b) compared wavelet and fast data sparse approximations for boundary - domain

integral equations of Poisson type.

2. Governing equations

In this work, we will present a numerical algorithm and simulation results for heat transfer in pure fluids and in nanofluids. We present the governing equations for nanofluids, since they can be, by choosing the correct parameter values, used for pure fluids as well. We assume the pure fluid and nanofluid to be incompressible. Flow in our simulations is laminar and steady. Effective properties of the nanofluid are: density ρ_{nf}, dynamic viscosity μ_{nf}, heat capacitance $(c_p)_{nf}$, thermal expansion coefficient β_{nf} and thermal conductivity k_{nf}, where subscript nf is used to denote effective i.e. nanofluid properties. The properties are all assumed constant throughout the flow domain. The mass conservation law for an incompressible fluid may be stated as

$$\vec{\nabla} \cdot \vec{v} = 0. \tag{1}$$

Considering constant nanofluid material properties and taking density variation into account within the Boussinesq approximation we write the momentum equation as

$$\frac{\partial \vec{v}}{\partial t} + (\vec{v} \cdot \vec{\nabla})\vec{v} = -\beta_{nf}(T - T_0)\vec{g} - \frac{1}{\rho_{nf}}\vec{\nabla} p + \frac{\mu_{nf}}{\rho_{nf}}\nabla^2 \vec{v}. \tag{2}$$

We assume that no internal energy sources are present in the fluid. We will not deal with high velocity flow of highly viscous fluid, hence we will neglect irreversible viscous dissipation. With this, the internal energy conservation law, written with temperature as the unknown variable, reads as:

$$\frac{\partial T}{\partial t} + (\vec{v} \cdot \vec{\nabla})T = \frac{k_{nf}}{(\rho c_p)_{nf}}\nabla^2 T. \tag{3}$$

Relationships between properties of nanofluid to those of pure fluid and pure solid are provided with the models. Density of the nanofluid is calculated using particle volume fraction φ and densities of pure fluid ρ_f and of solid nanoparticles ρ_s as:

$$\rho_{nf} = (1 - \varphi)\rho_f + \varphi\rho_s \tag{4}$$

The effective dynamic viscosity of a fluid of dynamic viscosity μ_f containing a dilute suspension of small rigid spherical particles, is given by Brinkman (1952) as

$$\mu_{nf} = \frac{\mu_f}{(1 - \varphi)^{2.5}}. \tag{5}$$

The effective viscosity is independent of nanoparticle type, thus the differences in heat transfer between different nanofluids will be caused by heat related physical parameters only. The heat capacitance of the nanofluid can be expressed as (Khanafer et al., 2003):

$$(\rho c_p)_{nf} = (1 - \varphi)(\rho c_p)_f + \varphi(\rho c_p)_s. \tag{6}$$

Similarly, the nanofluid thermal expansion coefficient can be written as $(\rho\beta)_{nf} = (1 - \varphi)(\rho\beta)_f + \varphi(\rho\beta)_s$, which may be, by taking into account the definition of ρ_{nf} in equation (4), written as:

$$\beta_{nf} = \beta_f \left[\frac{1}{1 + \frac{(1-\varphi)\rho_f}{\varphi\rho_s}} \frac{\beta_s}{\beta_f} + \frac{1}{1 + \frac{\varphi}{1-\varphi}\frac{\rho_s}{\rho_f}} \right]. \tag{7}$$

The effective thermal conductivity of the nanofluid is approximated by the Maxwell-Garnett formula

$$k_{nf} = k_f \frac{k_s + 2k_f - 2\varphi(k_f - k_s)}{k_s + 2k_f + \varphi(k_f - k_s)}. \tag{8}$$

This formula is valid only for spherical particles (Shukla & Dhir, 2005), since it does not take into account the shape of particles. Our macroscopic modelling of nanofluids is restricted to spherical nanoparticles and it is suitable for small temperature gradients.

2.1 Nondimensional equations in velocity-vorticity form

Vorticity, $\vec{\omega}$, is defined as a curl of velocity. By taking the curl of the mass conservation law (1) and of the momentum transport equation (2) and taking into account that by definition vorticity is solenodial, $\vec{\nabla} \cdot \vec{\omega} = 0$, we derive the velocity-vorticity formulation of Navier-Stokes equations. The equations are rewritten into nondimensional form using

$$\vec{v} \to \frac{\vec{v}}{v_0}, \vec{r} \to \frac{\vec{r}}{L}, \omega \to \frac{\omega L}{v_0}, t \to \frac{v_0 t}{L}, T \to \frac{T - T_0}{\Delta T}, \vec{g} \to \frac{\vec{g}}{g_0}, v_0 = \frac{k_f}{(\rho c_p)_f L}, \tag{9}$$

where T_0 and L are characteristic temperature and length scale. Characteristic temperature difference is ΔT, while $g_0 = 9.81 m/s^2$. We define pure fluid Rayleigh and Prandtl number values as

$$Ra = \frac{g_0 \beta_f \Delta T L^3 \rho_f (\rho c_p)_f}{\mu_f k_f}, \qquad Pr = \frac{\mu_f c_p}{k_f}. \tag{10}$$

The choice for characteristic velocity v_0 in (9) is common for buoyant flow simulations. It ensures that the Reynolds number is eliminated for the governing equations, since its value multiplied by Prandtl number equals one. With this the nondimensional velocity-vorticity formulation of Navier-Stokes equations for simulation of nanofluids consists of the kinematics equation, the vorticity transport equation and the energy equation:

$$\nabla^2 \vec{v} + \vec{\nabla} \times \vec{\omega} = 0, \tag{11}$$

$$\frac{\partial \vec{\omega}}{\partial t} + (\vec{v} \cdot \vec{\nabla})\vec{\omega} = (\vec{\omega} \cdot \vec{\nabla})\vec{v} + PrN_a \nabla^2 \vec{\omega} - PrRaN_b \vec{\nabla} \times T\vec{g}, \tag{12}$$

$$\frac{\partial T}{\partial t} + (\vec{v} \cdot \vec{\nabla})T = N_c \nabla^2 T, \tag{13}$$

$$N_a = \frac{\mu_{nf}}{\mu_f} \frac{\rho_f}{\rho_{nf}}, \qquad N_b = \frac{\beta_{nf}}{\beta_f}, \qquad N_c = \frac{k_{nf}}{k_f} \frac{(\rho c_p)_f}{(\rho c_p)_{nf}}. \tag{14}$$

The flow and heat transfer of a nanofluid is thus defined by specifying the pure fluid Rayleigh and Prandtl number values. The nanofluid properties are evaluated using the following models: ρ_{nf}/ρ_f from (4), μ_{nf}/μ_f from (5), $(\rho c_p)_{nf}/(\rho c_p)_f$ from (6), β_{nf}/β_f from (7) and k_{nf}/k_f from (8). The system of equations (11)-(13) can be used to simulate pure fluids by taking $N_a = N_b = N_c = 1$.

3. Numerical method

We will apply a combination of subdomain BEM and fast single domain BEM for the solution of the governing equations. The Dirichlet and/or Neumann boundary conditions for velocity and temperature are given. They are used to obtain solutions of the kinematics equation (11)

for domain velocity values and energy equation (13) for domain temperature values. The boundary conditions for vorticity, which are needed to solve the vorticity transport equation (12), are unknown. We will use the single domain BEM on the kinematics equation to obtain the unknown boundary vorticity values. The outline of the algorithm is as follows:

– initialization, calculate integrals
– begin nonlinear loop
  a) calculate boundary vorticity values by solving the kinematics equation (11) by fast single domain BEM (see section 3.4)
  a) calculate domain velocity values by solving the kinematics equation (11) by subdomain BEM (see section 3.3)
  a) solve the energy equation (3) using the new velocity field for domain temperature values by subdomain BEM (see section 3.2)
  a) solve vorticity transport equation (12) by subdomain BEM for domain vorticity values using the boundary values from the solution of the kinematics equation and new velocity and temperature fields (see section 3.1)
  a) check convergence - repeat steps in the nonlinear loop until convergence of all field functions is achieved
– end nonlinear loop

3.1 Subdomain BEM solution of the vorticity transport equation

Let us consider a domain Ω with a position vector $\vec{r} \in \mathbb{R}^3$. The boundary of the domain is $\Gamma = \partial\Omega$. In this work we are simulating steady flow fields, thus we may write $\partial\vec{\omega}/\partial t = 0$. The integral form of the steady vorticity transport equation (12) is (Wrobel, 2002):

$$c(\vec{\theta})\vec{\omega}(\vec{\theta}) + \int_\Gamma \vec{\omega}\vec{\nabla}u^\star \cdot \vec{n}d\Gamma = \int_\Gamma u^\star \vec{q}d\Gamma$$
$$+\frac{1}{PrN_a}\int_\Omega u^\star \left\{(\vec{v}\cdot\vec{\nabla})\vec{\omega} - (\vec{\omega}\cdot\vec{\nabla})\vec{v}\right\} d\Omega + Ra\frac{N_b}{N_a}\int_\Omega u^\star \vec{\nabla}\times T\vec{g}d\Omega, \tag{15}$$

where $\vec{\theta}$ is the source or collocation point, $\vec{n}$ is a vector normal to the boundary, pointing out of the domain and $u^\star$ is the fundamental solution for the diffusion operator:

$$u^\star = \frac{1}{4\pi|\vec{\theta}-\vec{r}|}. \tag{16}$$

$c(\vec{\theta})$ is the geometric factor defined as $c(\vec{\theta}) = \alpha/4\pi$, where α is the inner angle with origin in $\vec{\theta}$. If $\vec{\theta}$ lies inside of the domain then $c(\vec{\theta}) = 1$; $c(\vec{\theta}) = 1/2$, if $\vec{\theta}$ lies on a smooth boundary. Vorticity on the boundary $\vec{\omega}(\vec{r})$ or vorticity flux on the boundary $\vec{q}(\vec{r}) = \vec{\nabla}\vec{\omega}(\vec{r})\cdot\vec{n}$ can be prescribed as boundary conditions.

Both domain integrals on the right hand side of equation (15) include derivatives of the unknown field functions. In the following we will use algebraic relations to move the derivative from the unknown field function to the fundamental solution. Let us first write the first domain integral alone for j^{th} component of vorticity only:

$$\frac{1}{PrN_a}\int_\Omega \left\{(\vec{v}\cdot\vec{\nabla})\omega_j - (\vec{\omega}\cdot\vec{\nabla})v_j\right\} u^\star\Omega. \tag{17}$$

Due to the solenoidality of the velocity and vorticity fields, we may use $(\vec{\omega}\cdot\vec{\nabla})v_j = \vec{\nabla}\cdot(\vec{\omega}v_j)$ and $(\vec{v}\cdot\vec{\nabla})\omega_j = \vec{\nabla}\cdot(\vec{v}\omega_j)$ to transform eqaution (17) into

$$\frac{1}{PrN_a}\int_\Omega \left\{\vec{\nabla}\cdot(\vec{v}\omega_j - \vec{\omega}v_j)\right\} u^\star d\Omega. \tag{18}$$

In order to move the derivative towards the fundamental solution, the following algebraic relation $\vec{\nabla}\cdot\left\{u^*(\vec{v}\omega_j - \vec{\omega}v_j)\right\} = u^*\vec{\nabla}\cdot(\vec{v}\omega_j - \vec{\omega}v_j) + (\vec{v}\omega_j - \vec{\omega}v_j)\cdot\vec{\nabla}u^*$ is used to obtain two integrals

$$\frac{1}{PrN_a}\int_\Omega \vec{\nabla}\cdot\left\{u^*(\vec{v}\omega_j - \vec{\omega}v_j)\right\} d\Omega - \frac{1}{PrN_a}\int_\Omega (\vec{v}\omega_j - \vec{\omega}v_j)\cdot\vec{\nabla}u^\star d\Omega. \tag{19}$$

The first integral may be converted to a boundary integral using a Gauss divergence clause. Thus, the final form of the first domain integral of equation (15) for j^{th} vorticity component without derivatives of field functions may be stated as:

$$\frac{1}{PrN_a}\int_\Gamma \vec{n}\cdot\left\{u^*(\vec{v}\omega_j - \vec{\omega}v_j)\right\} d\Gamma - \frac{1}{PrN_a}\int_\Omega (\vec{v}\omega_j - \vec{\omega}v_j)\cdot\vec{\nabla}u^* d\Omega. \tag{20}$$

In order to remove the derivative of temperature from the second domain integral of equation (15), we make use of the following algebraic relation: $\vec{\nabla}\times(u^\star T\vec{g}) = u^\star\vec{\nabla}\times T\vec{g} + T\vec{\nabla}\times u^\star\vec{g}$, which gives

$$+ Ra\frac{N_b}{N_a}\int_\Omega \vec{\nabla}\times(u^\star T\vec{g})d\Omega - Ra\frac{N_b}{N_a}\int_\Omega T\vec{\nabla}\times u^\star\vec{g}d\Omega. \tag{21}$$

With the aid of the Gauss clause we are able to transform the first domain integral of equation (21) into a boundary integral:

$$- Ra\frac{N_b}{N_a}\int_\Gamma u^\star T\vec{g}\times\vec{n}d\Gamma - Ra\frac{N_b}{N_a}\int_\Omega T\vec{\nabla}\times u^\star\vec{g}d\Omega, \tag{22}$$

yielding an expression without derivatives of the temperature field. Using expressions (20) and (22) instead of the domain integrals in equation (15), we may write the final integral form of the vorticity transport equation as:

$$\begin{aligned} c(\vec{\theta})\omega_j(\vec{\theta}) + \int_\Gamma \omega_j\vec{\nabla}u^*\cdot\vec{n}d\Gamma &= \int_\Gamma u^* q_j d\Gamma \\ + \frac{1}{PrN_a}\int_\Gamma \vec{n}\cdot\left\{u^*(\vec{v}\omega_j - \vec{\omega}v_j)\right\} d\Gamma - \frac{1}{PrN_a}\int_\Omega (\vec{v}\omega_j - \vec{\omega}v_j)\cdot\vec{\nabla}u^* d\Omega & \\ -Ra\frac{N_b}{N_a}\int_\Gamma (u^\star T\vec{g}\times\vec{n})_j d\Gamma - Ra\frac{N_b}{N_a}\int_\Omega (T\vec{\nabla}\times u^\star\vec{g})_j d\Omega. \end{aligned} \tag{23}$$

In the subdomain BEM method we make a mesh of the entire domain Ω and name each mesh element a subdomain. Equation (23) is written for each of the subdomains. In order to obtain a discrete version of (23) we use shape functions to interpolate field functions and flux. We used hexahedral subdomains with 27 nodes, which enable continuous quadratic interpolation of field functions. On each boundary element we interpolate the flux using discontinuous linear interpolation scheme with 4 nodes. By using discontinuous interpolation we avoid flux definition problems in corners and edges. A subdomain and one boundary element are sketched in Figure 1. A function, e.g. temperature, is interpolated over a boundary elements

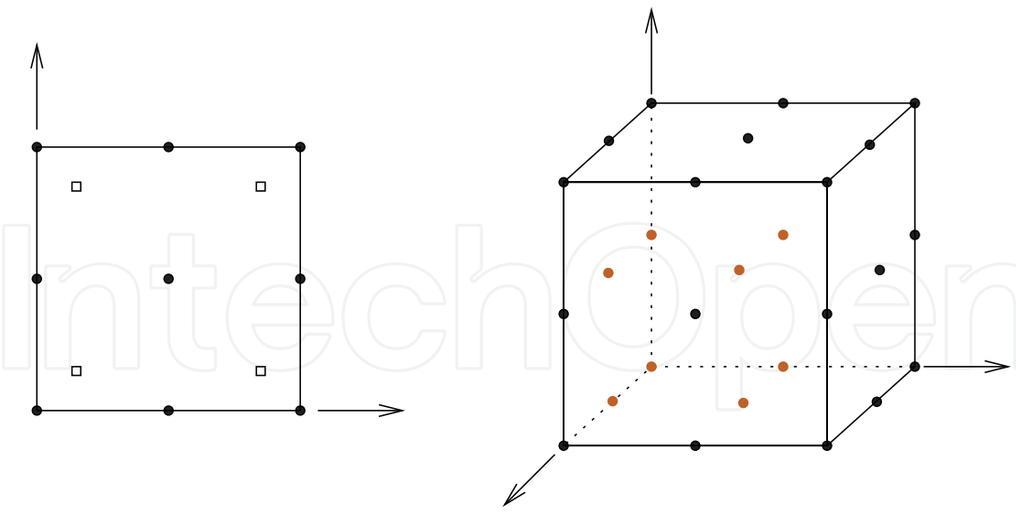

Fig. 1. A boundary element with function (circles) and flux (squares) nodes is shown on the left. A hexahedral subdomain with function nodes is shown on the right.

as $T = \sum \varphi_i T_i$, inside each subdomain as $T = \sum \Phi_i T_i$, while flux is interpolated over boundary elements as $q = \sum \phi_i q_i$.
The following integrals must be calculated:

$$[H] = \int_\Gamma \varphi_i \vec{\nabla} u^\star \cdot \vec{n} d\Gamma, \quad [G] = \int_\Gamma \phi_i u^\star d\Gamma, \quad [\vec{A}] = \int_\Gamma \varphi_i \vec{n} u^\star d\Gamma, \quad [\vec{D}] = \int_\Omega \Phi_i \vec{\nabla} u^\star d\Omega. \tag{24}$$

The square brackets denote integral matrices. Each source point location yields one row in these matrices. In order to calculate the integrals, a Gaussian quadrature algorithm is used. Calculation of the free coefficient $c(\vec{\theta})$ is preformed indirectly using a rigid body movement solution. The calculated $c(\vec{\theta})$ are added to the diagonal terms of the $[H]$ matrix.
The source point is set to all function and flux nodes in each subdomain. That makes the number of rows of each matrix 51 times the number of subdomains. By letting curly brackets denote vectors of nodal values of field functions, we may write the discrete vorticity transport equation in component form as:

$$\begin{aligned}[H]\{\omega_x\} = [G]\{q_x\} &+ \frac{1}{PrN_a}[A_y]\{v_y\omega_x - \omega_y v_x\} + \frac{1}{PrN_a}[A_z]\{v_z\omega_x - \omega_z v_x\} \\ &- \frac{1}{PrN_a}[D_y]\{v_y\omega_x - \omega_y v_x\} - \frac{1}{PrN_a}[D_z]\{v_z\omega_x - \omega_z v_x\} \\ &+ Ra\frac{N_b}{N_a}\left(g_z[A_y]\{T\} - g_y[A_z]\{T\} - g_z[D_y]\{T\} + g_y[D_z]\{T\}\right),\end{aligned} \tag{25}$$

$$\begin{aligned}[H]\{\omega_y\} = [G]\{q_y\} &+ \frac{1}{PrN_a}[A_x]\{v_x\omega_y - \omega_x v_y\} + \frac{1}{PrN_a}[A_z]\{v_z\omega_y - \omega_z v_y\} \\ &- \frac{1}{PrN_a}[D_x]\{v_x\omega_y - \omega_x v_y\} - \frac{1}{PrN_a}[D_z]\{v_z\omega_y - \omega_z v_y\} \\ &+ Ra\frac{N_b}{N_a}\left(g_x[A_z]\{T\} - g_z[A_x]\{T\} + g_z[D_x]\{T\} - g_x[D_z]\{T\}\right),\end{aligned} \tag{26}$$

$$[H]\{\omega_z\} = [G]\{q_z\} + \frac{1}{PrN_a}[A_x]\{v_x\omega_z - \omega_x v_z\} + \frac{1}{PrN_a}[A_y]\{v_y\omega_z - \omega_y v_z\}$$
$$- \frac{1}{PrN_a}[D_x]\{v_x\omega_z - \omega_x v_z\} - \frac{1}{PrN_a}[D_y]\{v_y\omega_z - \omega_y v_z\}$$
$$+Ra\frac{N_b}{N_a}\left(g_y[A_x]\{T\} - g_x[A_y]\{T\} - g_y[D_x]\{T\} + g_x[D_y]\{T\}\right). \quad (27)$$

Since neighbouring subdomains share nodes, the systems of linear equations (25), (26) and (27) are over-determined. After taking into account the boundary conditions, we solve them using a least squares solver (Paige & Saunders, 1982).

3.2 Subdomain BEM solution of the energy equation

The energy equation (13) is also of a diffusion convection type. The solution of (13) is thus obtained in the same manner than the solution of the vorticity transfer equation. The discrete counterpart of the energy equation (13) is:

$$[H]\{T\} = [G]\{q_T\} +$$
$$+\frac{1}{N_c}\left([A_x]\{v_x T\} + [A_y]\{v_y T\} + [A_z]\{v_z T\} - [D_x]\{v_x T\} - [D_y]\{v_y T\} - [D_z]\{v_z T\}\right), \quad (28)$$

where $\{q_T\}$ is a nodal vector of temperature flux. Boundary conditions are either known temperature or temperature flux on the boundary. The system matrix is sparse and as such it is stored efficiently in a compressed row storage format. The system is solved in a least squares manner (Paige & Saunders, 1982).

3.3 Subdomain BEM solution of the kinematics equation

The kinematics equation (11) is an elliptic Poisson type equation. Its integral form (Wrobel, 2002) is

$$c(\xi)\vec{v}(\xi) + \int_\Gamma \vec{v}(\vec{n}\cdot\vec{\nabla})u^\star d\Gamma = \int_\Gamma u^\star(\vec{n}\cdot\vec{\nabla})\vec{v}d\Gamma + \int_\Omega(\vec{\nabla}\times\vec{\omega})u^\star d\Omega, \quad \xi\in\Gamma \quad (29)$$

The domain integral on the right hand side of equation (29) includes derivatives of vorticity. The equation is reformulated to transfer the derivative from the vorticity to the fundamental solution. We use the the definition of a curl of a product, i.e. $\vec{\nabla}\times(\vec{\omega}u^\star) = (\vec{\nabla}\times\vec{\omega})u^\star - \vec{\omega}\times\vec{\nabla}u^\star$ and obtain

$$\int_\Omega(\vec{\nabla}\times\vec{\omega})u^\star d\Omega = \int_\Omega(\vec{\nabla}\times(\vec{\omega}u^\star))d\Omega + \int_\Omega(\vec{\omega}\times\vec{\nabla}u^\star)d\Omega. \quad (30)$$

Using a derived form of the Gauss divergence clause, $\int_\Omega\vec{\nabla}\times\vec{F}d\Omega = -\int_\Gamma\vec{F}\times\vec{n}d\Gamma$, to change the first domain integral on the right hand side of (30) into a boundary integral, yields

$$\int_\Omega(\vec{\nabla}\times\vec{\omega})u^\star d\Omega = -\int_\Gamma(\vec{\omega}u^\star)\times\vec{n}d\Gamma + \int_\Omega(\vec{\omega}\times\vec{\nabla}u^\star)d\Omega. \quad (31)$$

Equation (31) is inserted into (29) and a new integral form of kinematics equation is obtained

$$c(\xi)\vec{v}(\xi) + \int_\Gamma\vec{v}(\vec{n}\cdot\vec{\nabla})u^\star d\Gamma = \int_\Gamma u^\star\left\{(\vec{n}\cdot\vec{\nabla})\vec{v} - \vec{\omega}\times\vec{n}\right\}d\Gamma + \int_\Omega(\vec{\omega}\times\vec{\nabla}u^\star)d\Omega. \quad (32)$$

The term in curly brackets in the boundary integral on the right hand side of equation (32) is for solenoidal fluid equal to $(\vec{n}\cdot\vec{\nabla})\vec{v}-\vec{\omega}\times\vec{n}=(\vec{n}\times\vec{\nabla})\times\vec{v}$. Using this relationship in equation (32) one can further rewrite the boundary integral as

$$\int_\Gamma u^\star(\vec{n}\times\vec{\nabla})\times\vec{v}d\Gamma=\int_\Gamma(\vec{n}\times\vec{\nabla})\times(\vec{v}u^\star)d\Gamma+\int_\Gamma\vec{v}\times(\vec{n}\times\vec{\nabla})u^\star d\Gamma \tag{33}$$

The first integral on the right hand side of the above equation represents an integral over a closed surface of a tangential derivative of a vector function. For a continuous function, such integral is always equal to zero. Inserting equation (33) into (32) we obtain an integral kinematics equation without derivatives of the velocity or vorticity fields:

$$c(\xi)\vec{v}(\xi)+\int_\Gamma\vec{v}(\vec{n}\cdot\vec{\nabla})u^\star d\Gamma=\int_\Gamma\vec{v}\times(\vec{n}\times\vec{\nabla})u^\star d\Gamma+\int_\Omega(\vec{\omega}\times\vec{\nabla}u^\star)d\Omega. \tag{34}$$

The boundary integrals on the left hand side are stored in the $[H]$ matrix, the domain integrals on the right hand side are the $[\vec{D}]$ matrices. We define the boundary integral on the right hand side as $[\vec{H}^t]$ integrals in the following manner:

$$[\vec{H}^t]=\int_\Gamma\varphi_i(\vec{n}\times\vec{\nabla})u^\star d\Gamma. \tag{35}$$

Since there are no fluxes in the equation, the source point is set to function nodes only. The discrete kinematics equation written in component wise form is:

$$[H]\{v_x\}=[H_z^t]\{v_y\}-[H_y^t]\{v_z\}+[D_z]\{\omega_y\}-[D_y]\{\omega_z\}, \tag{36}$$

$$[H]\{v_y\}=[H_x^t]\{v_z\}-[H_z^t]\{v_x\}-[D_z]\{\omega_x\}+[D_x]\{\omega_z\}, \tag{37}$$

$$[H]\{v_z\}=[H_y^t]\{v_x\}-[H_x^t]\{v_y\}+[D_y]\{\omega_x\}-[D_x]\{\omega_y\}. \tag{38}$$

The kinematics equation takes the same form for fluid flow problems and for coupled fluid flow - heat transfer problems. This form is used on every subdomain of the mesh to evaluate velocity flow field.

3.4 Fast Single domain BEM solution of the kinematics equation

In order to use the kinematics equation to obtain boundary vorticity values, we must rewrite the equation (34) in a tangential form by multiplying the system with a normal in the source point $\vec{n}(\vec{\theta})$:

$$\begin{aligned}c(\vec{\theta})\vec{n}(\vec{\theta})\times\vec{v}(\vec{\theta})+\vec{n}(\vec{\theta})\times\int_\Gamma\vec{v}\vec{\nabla}u^\star\cdot\vec{n}d\Gamma\\ =\vec{n}(\vec{\theta})\times\int_\Gamma\vec{v}\times(\vec{n}\times\vec{\nabla})u^\star d\Gamma+\vec{n}(\vec{\theta})\times\int_\Omega(\vec{\omega}\times\vec{\nabla}u^\star)d\Omega.\end{aligned} \tag{39}$$

This approach has been proposed by Škerget and used in 2D by Škerget et al. (2003) and in 3D by Žunič et al. (2007) and Ravnik et al. (2009a). The discrete form of the equations is

$$\begin{aligned}\{n_y\}[H]\{v_z\}-\{n_z\}[H]\{v_y\}=\{n_y\}([H_y^t]\{v_x\}-[H_x^t]\{v_y\}+[D_y]\{\omega_x\}-[D_x]\{\omega_y\})-\\ -\{n_z\}([H_x^t]\{v_z\}-[H_z^t]\{v_x\}-[D_z]\{\omega_x\}+[D_x]\{\omega_z\}),\end{aligned} \tag{40}$$

$$\{n_z\}[H]\{v_x\} - \{n_x\}[H]\{v_z\} = \{n_z\}([H_z^t]\{v_y\} - [H_y^t]\{v_z\} + [D_z]\{\omega_y\} - [D_y]\{\omega_z\}) - \\ -\{n_x\}([H_y^t]\{v_x\} - [H_x^t]\{v_y\} + [D_y]\{\omega_x\} - [D_x]\{\omega_y\}), \quad (41)$$

$$\{n_x\}[H]\{v_y\} - \{n_y\}[H]\{v_x\} = \{n_x\}([H_x^t]\{v_z\} - [H_z^t]\{v_x\} - [D_z]\{\omega_x\} + [D_x]\{\omega_z\}) - \\ -\{n_y\}([H_z^t]\{v_y\} - [H_y^t]\{v_z\} + [D_z]\{\omega_y\} - [D_y]\{\omega_z\}). \quad (42)$$

In order to write a system of equations for boundary vorticity, we decompose the vorticity nodal vectors in two parts. In the boundary part $\{\omega_i^\Gamma\}$ only boundary nodes are included, in the domain part $\{\omega_i^{\Omega\setminus\Gamma}\}$ the domain nodes are listed. The corresponding columns of the domain integral matrices are also separated into boudnary $[D_i^\Gamma]$ and domain $[D_i^{\Omega\setminus\Gamma}]$ parts. With this, the final form of the system of equation for the unknown boundary vorticity $\{\omega_x^\Gamma\}$, $\{\omega_y^\Gamma\}$, $\{\omega_z^\Gamma\}$ is

$$(\{n_x\}[D_x^\Gamma] + \{n_y\}[D_y^\Gamma] + \{n_z\}[D_z^\Gamma])\{\omega_x^\Gamma\} = \\ \{n_x\}[D_x^\Gamma]\{\omega_x^\Gamma\} - \{n_y\}[D_y^{\Omega\setminus\Gamma}]\{\omega_x^{\Omega\setminus\Gamma}\} - \{n_z\}[D_z^{\Omega\setminus\Gamma}])\{\omega_x^{\Omega\setminus\Gamma}\} + \\ \{n_y\}[H]\{v_z\} - \{n_z\}[H]\{v_y\} - \{n_y\}([H_y^t]\{v_x\} - [H_x^t]\{v_y\} - [D_x]\{\omega_y\}) + \\ \{n_z\}([H_x^t]\{v_z\} - [H_z^t]\{v_x\} + [D_x]\{\omega_z\}), \quad (43)$$

$$(\{n_x\}[D_x^\Gamma] + \{n_y\}[D_y^\Gamma] + \{n_z\}[D_z^\Gamma])\{\omega_y^\Gamma\} = \\ \{n_y\}[D_y^\Gamma]\{\omega_y^\Gamma\} - \{n_z\}[D_z^{\Omega\setminus\Gamma}]\{\omega_y^{\Omega\setminus\Gamma}\} - \{n_x\}[D_x^{\Omega\setminus\Gamma}])\{\omega_y^{\Omega\setminus\Gamma}\} + \\ \{n_z\}[H]\{v_x\} - \{n_x\}[H]\{v_z\} - \{n_z\}([H_z^t]\{v_y\} - [H_y^t]\{v_z\} - [D_y]\{\omega_z\}) + \\ \{n_x\}([H_y^t]\{v_x\} - [H_x^t]\{v_y\} + [D_y]\{\omega_x\}), \quad (44)$$

$$(\{n_x\}[D_x^\Gamma] + \{n_y\}[D_y^\Gamma] + \{n_z\}[D_z^\Gamma])\{\omega_z^\Gamma\} = \\ \{n_z\}[D_z^\Gamma]\{\omega_z^\Gamma\} - \{n_x\}[D_x^{\Omega\setminus\Gamma}]\{\omega_z^{\Omega\setminus\Gamma}\} - \{n_y\}[D_y^{\Omega\setminus\Gamma}])\{\omega_z^{\Omega\setminus\Gamma}\} + \\ \{n_x\}[H]\{v_y\} - \{n_y\}[H]\{v_x\} - \{n_x\}([H_x^t]\{v_z\} - [H_z^t]\{v_x\} - [D_z]\{\omega_x\}) + \\ \{n_y\}([H_z^t]\{v_y\} - [H_y^t]\{v_z\} + [D_z]\{\omega_y\}). \quad (45)$$

We set the source point into every boundary node of the whole computational domain. This yields a full system matrix with number of boundary nodes rows and columns. It is solved using a LU decomposition method. The domain matrices have the number of columns equal to the number of domain nodes. In order to reduce storage requirements and to make algebraic operation with domain matrices fast, we introduce a kernel expansion based approximation technique (Ravnik et al., 2009c).

3.4.1 Series expansion

The approximation method is based on the fact that it is possible to separate the variables (i.e. the collocation point $\vec{\theta}$ and the domain integration point $\vec{r}$) of the integral kernel of equation

(24) by series expansion. The gradient of the Laplace fundamental solution is expanded into a spherical harmonics series in the following manner:

$$\vec{\nabla}u^{\star} = \sum_{l=0}^{\infty}\sum_{m=-l}^{l}\frac{(-1)^m}{2l+1}\frac{1}{\xi^{l+1}}Y_l^{-m}(\theta_\xi,\varphi_\xi)\left\{lY_l^m(\theta_r,\varphi_r)r^{l-2}\vec{r}+r^l\vec{\nabla}Y_l^m(\theta_r,\varphi_r)\right\}, \tag{46}$$

where Y_l^m are spherical harmonics in polar coordinate system; $\vec{r}=(r,\varphi_r,\theta_r)$ and $\vec{\theta}=(\xi,\varphi_\xi,\theta_\xi)$. The gradient of spherical harmonics is expressed using associated Legendre polynomials P_l^m as

$$\vec{\nabla}Y_l^m(\theta,\varphi) = \sqrt{\frac{2l+1}{4\pi}\frac{(l-m)!}{(l+m)!}}\vec{\nabla}\left\{P_l^m(\cos\theta)\frac{\partial e^{im\varphi}}{\partial\varphi}\vec{\nabla}\varphi-\sin(\theta)\frac{\partial P_l^m(\cos\theta)}{\partial\cos\theta}\vec{\nabla}\theta\right\}. \tag{47}$$

The associated Legendre polynomials are evaluated using recurrence relations as described in Press et al. (1997). The derivatives of associated Legendre polynomials are obtained using the following recurrence relation:

$$\frac{\partial P_l^m(x)}{\partial x} = \frac{lxP_l^m(x)-(l+m)P_{l-1}^m(x)}{x^2-1}. \tag{48}$$

The derivatives of the polar angles written in Cartesian coordinate system are

$$\vec{\nabla}\theta = \frac{\sqrt{x^2+y^2}}{x^2+y^2+z^2}\left(\frac{zx}{x^2+y^2},\frac{zy}{x^2+y^2},-1\right), \qquad \vec{\nabla}\varphi = \frac{1}{x^2+y^2}(-y,x,0). \tag{49}$$

The origin of the coordinate system is set in such locations that the series convergence is improved. Using the above expansion, the domain integrals of equation (24) may now be written with separate variables. We are able to approximately calculate each entry in the domain matrices with the above sum. The number of expansion terms $n_{exp}=(L+1)^2$ in the series controls the accuracy of the approximation. Using the series instead of the direct evaluation of the integral kernel does not by itself bring a reduction of memory. Only when the expansion is used on a cluster of collocation points and domain cells it is possible to form a data sparse approximation of a part of the domain matrix. The clusters are formed and organized in a hierarchical tree-like structure, which is described below.

3.4.2 Cluster trees

Let us consider a cluster of n_r nearby collocation points and a cluster of n_c nearby domain cells, as illustrated in Figure 2.

These correspond to a $n_r \times n_c$ matrix block, which is a part of the domain matrix. Since the variables in the series are separated, it is possible to evaluate two lower order matrix blocks ($n_r \times n_{exp}$) and ($n_{exp} \times n_c$) instead of the full matrix block ($n_r \times n_c$). In the first lower order matrix block expansion terms that depend on source point location are evaluated for all collocation points. In the second one integrals of expansion terms that depend on domain location are evaluated for all domain cells. Multiplication of the two lower order matrix blocks gives the full $n_r \times n_c$ matrix block up to an expansion error. This technique saves memory if the amount of data, that must be stored in the two lower order matrices, is smaller than the amount of data in the full matrix block. As long as the collocation node cluster and the domain cells cluster are far apart this technique can be used. When the clusters coincide, i.e. the collocation nodes are a part of the integration cells, the kernels are singular. Such

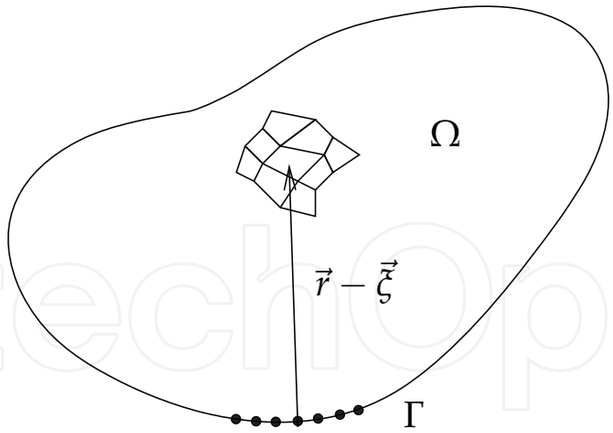

Fig. 2. A problem domain shown with a cluster of collocation points $\vec{\theta}$ and a cluster of domain cells.

cluster pairs are called inadmissible and the corresponding matrix block is evaluated in full, not approximated with two lower order matrices.

We constructed a tree of collocation point clusters and a tree of clusters of domain cells. The trees were constructed in a recursive hierarchical manner. The problem domain was enclosed by a parallelepiped. The parallelepiped is cut in half by a plane, breaking the root clusters into two. The cutting process is repeated recursively, so the clusters on each level have less and less collocation points and domain cells. The cutting sequence is stopped, when memory can no longer be saved.

Each branch of the collocation tree is paired with each branch of the domain cells tree on the same level and with each branch of the domain cells tree on the next level thus forming branches on the tree of pairs of clusters. For each pair a decision is taken based on the admissibility criterion whether a sparse approximation for this cluster pair is possible or not. If the pair is admissible, the branch on the tree becomes an admissible leaf, where the two low order matrices will be calculated. If admissibility criterion is not reached until the last level of the tree, such cluster pairs are inadmissible and will be calculated in full and not with the sparse approximation.

To illustrate the algorithm, a cubic domain is considered meshed by 12^3 domain cells having in total 25^3 nodes. Admissible and inadmissible blocks are shown in Figure 3.

4. Test cases

The developed numerical scheme was used to simulate fluid flow and heat transfer of pure fluids and nanofluids. Two configurations were considered: the hotstrip and the differentially heated cavity. Sketches and boundary conditions for both cases are shown in Figure 4.

Applying a temperature difference on two opposite walls of an otherwise insulated cavity starts up natural convection producing a large vortex in the main part of the cavity. At low Rayleigh number values the vortex is weak and the heat is transferred predominately with conduction. Convection dominates at $Ra = 10^6$ where temperature stratification may be observed. The flow becomes unsteady for higher Ra values with vortices forming along the hot and cold walls. Natural convection of air and other pure fluids in a differentially heated cavity has been under intense investigation in the past. Recently several authors simulated

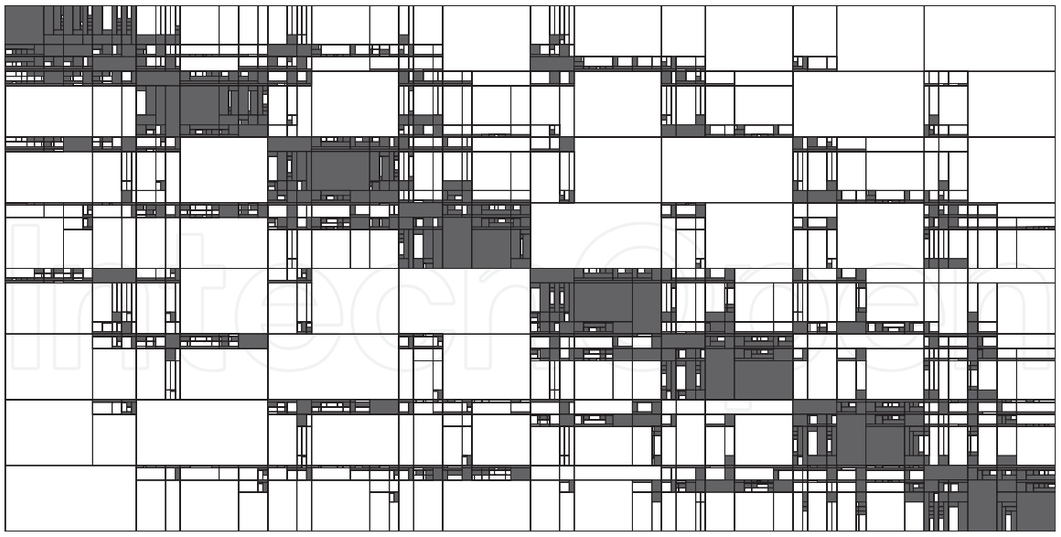

Fig. 3. Matrix structure of a cubic mesh (12^3 cells, 25^3 nodes). Filled areas show inadmissible matrix blocks, white areas are admissible matrix blocks obtained using an admissibility criteria of $\epsilon = 10^{-4}$.

nanofluids in this case (Abu-Nada & Oztop, 2009; Hwang et al., 2007; Ho et al., 2008; Tiwari & Das, 2007; Ravnik et al., 2010).
The hotstrip heats the surrounding fluid inducing two large main vortices. When the hotstrip is located in the centre of the cavity, the flow field is symmetric and the fluid rises from the centre of the hotstrip. If the hotstrip is placed off-centre, the flow symmetry is lost. Corvaro & Paroncini (2009; 2008) performed a 2D PIV experiment on a hotstrip problem, using air as the working fluid. Simulations of natural convection around the hotstrip were presented by Ravnik & Škerget (2009) and Ravnik et al. (2010).

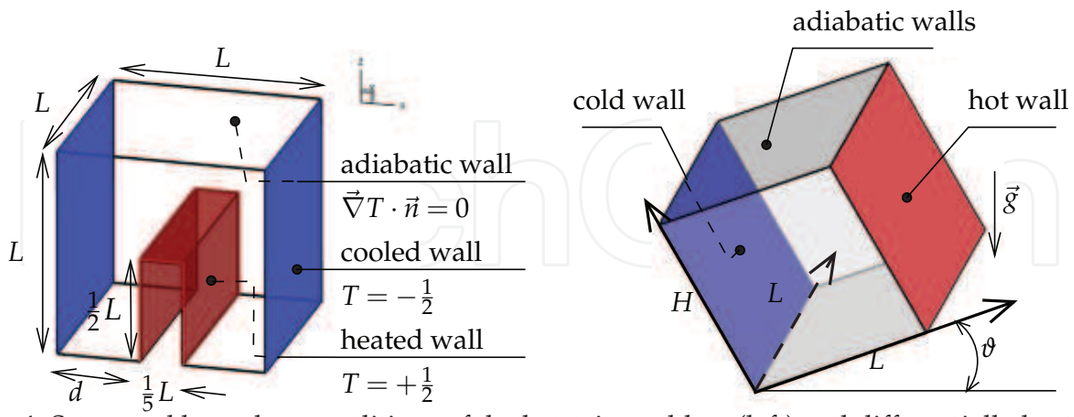

Fig. 4. Setup and boundary conditions of the hotstrip problem (left) and differentially heated cavity problem (right). Hotstrip of height $0.5L$ and width $0.2L$ is located at distance d from the left cold wall. The hotstrip is heated to $T = +0.5$, while the walls at $x = 0$ and $x = L$ are cooled to $T = -0.5$. There is no temperature flux through all other walls. In differentially heated cavity we keep two opposite vertical walls cold and hot, while all other walls are adiabatic. The height of the cavity is H, while its width and length are L. No-slip velocity boundary conditions are applied on all walls.

Both cases were investigated for air ($Pr = 0.71$), water ($Pr = 6.2$) and water based nanofluids (Table 1) for several Rayleigh number values. The hotstrip was positioned in the centre of the cavity ($d = 0.4H$) and off-centre ($d = 0.5H$). Aspect ratio of the differentially heated cavity was $H/L = 1$ and $H/L = 2$.
Normally, the heat flux $\dot{Q}$ is expressed in terms of pure fluid thermal conductivity, characteristic flow scales and a nondimensional Nusselt number, i.e. $\dot{Q} = k_f L \Delta T \cdot Nu$. The Nusselt number, Nu, is defined as the integral of the temperature flux through a wall. For a nanofluid, it is written as

$$Nu = \frac{k_{nf}}{k_f} \frac{1}{\Gamma_0} \int_{\Gamma} \vec{\nabla} T \cdot \vec{n} d\Gamma, \tag{50}$$

where Γ is the surface through which we calculate the heat flux and $\vec{n}$ is a unit normal to this surface. The area of the surface is Γ_0. The same definition may be used to pure fluids, since there $k_{nf}/k_f = 1$.

4.1 Natural convection in a differentially heated cavity

The domain was discretizised using 41^3 nodes. Nodes were concentrated towards the hot and cold walls in such a way that the ratio between the largest and the smallest element length was 7. First, we examine the flow structure with air as the working fluid. Figure 5 shows temperature contour plots on the $y = 0.5$ plane for Rayleigh number $Ra = 10^5$ and different inclination angles for cubic and $H/L = 2$ cavity. We observe temperature stratification in all cases. When the cavity is inclined, the thermal boundary layers widen and the heat transfer decreases. Tables 2 and 3 provide the Nusselt number values. We observe a decrease of the values with increasing inclination angle and an increase of heat transfer with increasing Rayleigh number. Present values compare well with the solution provided by Lo et al. (2007) and Tric et al. (2000). Nusselt number values for $H/L = 2$ cavity are given in Table 4.
Comparison of pure fluids and nanofluids is given in Figure 6, where temperature contours for water and water based nanofluids on the central $y = 0.5L$ plane are shown. Two solid volume fractions are compared. We observe that the change in nano particle volume fraction changes the temperature field considerably, thus changing the heat transfer. Nusselt number values for the natural convection of nanofluids in a cubical cavity are given in Table 5. Using water based nanofluids instead of pure water increases heat transfer in all cases. For low Rayleigh number, where conduction is the predominant heat transfer mechanism, the enhancement is the largest. For Cu nanofluid at $Ra = 10^3$ we observe an 27.2% increase in heat transfer for $\varphi = 0.1$ and 64.1% for $\varphi = 0.2$. TiO_2 nanofluid exhibits lower heat transfer enhancement, since its thermal conductivity is lower than that of Cu and Al_2O_3 nanofluids. Al_2O_3 and Cu nanofluid exhibit approximately the same heat transfer enhancement. As the Rayleigh number increases, convection becomes the dominant heat transfer mechanism, while conduction is negligible. Thus, the increased thermal conductivity of nanofluids plays a less important role in the overall heat balance. All nanofluids exhibit smaller heat transfer

	pure water	Cu	Al_2O_3	TiO_2
$c_p[J/kgK]$	4179	385	765	686.2
$\rho[kg/m^3]$	997.1	8933	3970	4250
$k[W/mK]$	0.613	400	40	8.9538
$\beta[\cdot 10^{-5} K^{-1}]$	21	1.67	0.85	0.9
$\alpha[\cdot 10^{-7} m^2/s]$	1.47	1163	131.7	30.7

Table 1. Thermophysical properties of water based nanofluids (Oztop & Abu-Nada, 2008).

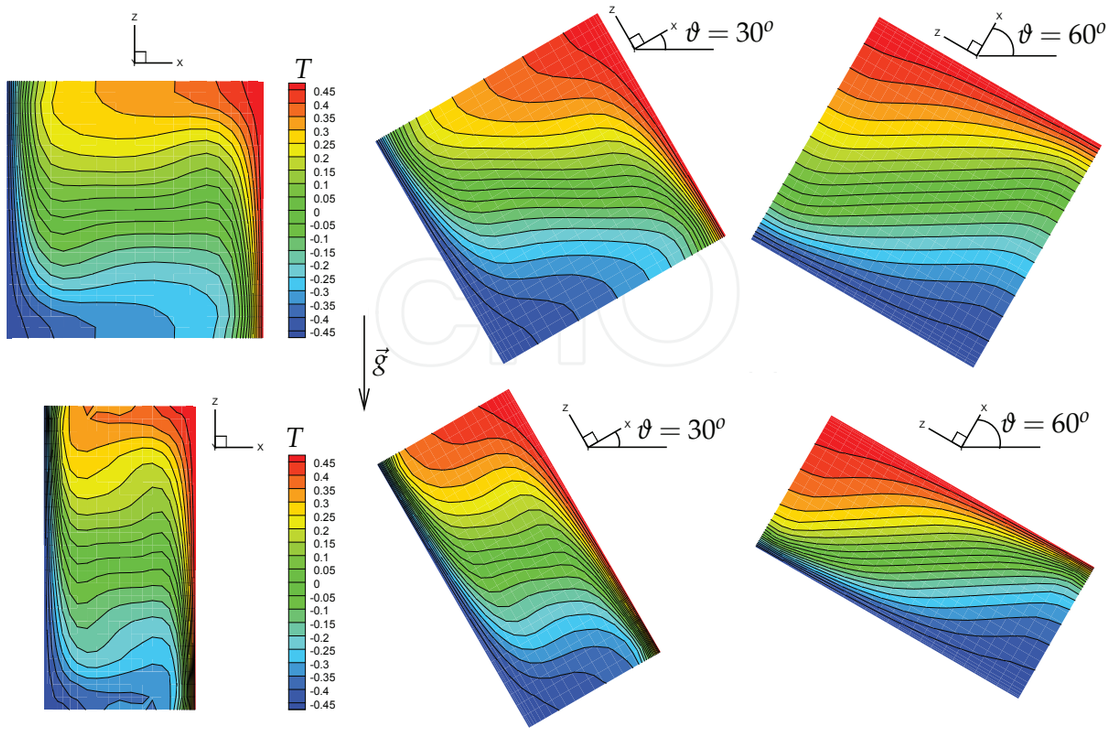

Fig. 5. Natural convection of air in a differentaily heat cavity. Temperature contour plots on the $y = 0.5$ plane for Rayleigh number $Ra = 10^5$; $\vartheta = 0^o$ (left), $\vartheta = 15^o$ (middle) and $\vartheta = 30^o$ (right). Top row: cubic cavity, bottom row $H/L = 2$ cavity. Gravity points downward in all cases.

enhancement as compared to the low Rayleigh number case. At $Ra = 10^6$ Cu nanofluid increases heat transfer at $\varphi = 0.1$ for 11.6% and at $\varphi = 0.2$ for 21.6%.

4.2 Natural convection around a hotstrip

Natural convection of air, water and water based nanofluids was simulated around the hotstrip. Two position of the hotstrip were considered - in the centre of the cavity ($d = 0.4L$) and off-centre ($d = 0.5L$). The mesh used for simulation had $61 \times 49 \times 19$ nodes in hexahedral cells. The nodes were concentrated towards the hot and cold walls.
Looking at the flow field of air in Figures 7 and 8 we observe that the hotstrip heats the surrounding fluid inducing two main vortices - one on each side. Hot fluid from the sides of the hotstrip is transported upwards by convection making the thermal boundary layer thin

	Air			Water
Ra	Lo et al. (2007)	Tric et al. (2000)	present	present
10^3	1.0710	1.0700	1.0712	1.071
10^4	2.0537	2.0542	2.0564	2.078
10^5	4.3329	4.3371	4.3432	4.510
10^6	8.6678	8.6407	8.6792	9.032

Table 2. Natural convection of air and water in a cubic cavity without inclination, $\vartheta = 0$. Present Nusselt number values are compared with the benchmark results of Lo et al. (2007) and Tric et al. (2000).

ϑ	Lo et al. (2007)			present		
	$Ra = 10^3$	$Ra = 10^4$	$Ra = 10^5$	$Ra = 10^3$	$Ra = 10^4$	$Ra = 10^5$
15^o	1.0590	1.8425	3.7731	1.0592	1.8464	3.7881
30^o	1.0432	1.5894	2.9014	1.0433	1.5916	2.9071
45^o	1.0268	1.3434	1.9791	1.0268	1.3443	1.9782
60^o	1.0127	1.1524	1.3623	1.0127	1.1526	1.3600

Table 3. Natural convection of air in a cubic cavity under inclination ϑ. Present Nusselt number values are compared with the benchmark results of Lo et al. (2007).

and thus resulting in high heat transfer. Upon reaching the top of the hotstrip the fluid flows over the top ultimately colliding with the fluid from the other side and rising upwards. When the hotstrip is located in the centre of the cavity, the flow field is symmetric and the fluid rises from the centre of the hotstrip. If the hotstrip is placed off-centre, the flow symmetry is lost. The sizes of large vortices on each side of the hotstrip are different. The flow does not rise above the centre of the hotstrip. Mixing of the fluid from both sides of the hotstrip occurs, which does not happen in the symmetric case.

We measured heat transfer in terms of the Nusselt number values over the whole surface of the hostrip (two vertical wall and a top wall). The values are shown in Table 6 for Rayleigh number values ranging from $Ra = 10^3$ to $Ra = 10^5$. We observe that the addition of nanoparticles increases heat transfer in all cases. The increase is the largest in the low Rayleigh number case and the smallest in the case of high Rayleigh values. This is expected, since at low Rayleigh number values conduction is the dominating heat transfer mechanism

ϑ	$Ra = 10^3$	$Ra = 10^4$	$Ra = 10^5$
0^o	1.111	2.163	4.177
15^o	1.096	2.029	3.892
30^o	1.073	1.839	3.430
45^o	1.047	1.594	2.774
60^o	1.023	1.317	1.915

Table 4. Natural convection of air in a $H/L = 2$ cavity. The Nusselt number values representing the heat flux through walls are shown for different inclination angles and Rayleigh numbers.

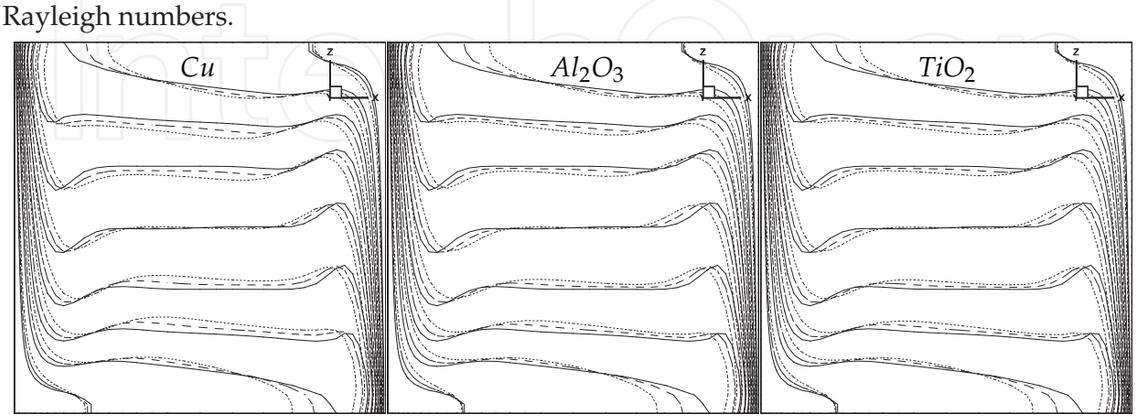

Fig. 6. Temperature contours on the central $y = 0.5H$ plane for natural convection in a differentially heated cubic cavity. Contour values are -0.4(0.1)0.4; $Ra = 10^6$. Solid line denotes pure water, dashed line $\varphi = 0.1$ nanofluid and dotted line $\varphi = 0.2$ nanofluid.

Ra	Water+Cu		Water+Al_2O_3		Water+TiO_2	
	$\varphi = 0.1$	$\varphi = 0.2$	$\varphi = 0.1$	$\varphi = 0.2$	$\varphi = 0.1$	$\varphi = 0.2$
10^3	1.363	1.758	1.345	1.718	1.297	1.598
10^4	2.237	2.381	2.168	2.244	2.115	2.132
10^5	4.946	5.278	4.806	4.968	4.684	4.732
10^6	10.08	10.98	9.817	10.39	9.556	9.871

Table 5. Nusselt number values for the natural convection of nanofluids in a cubical cavity. Solid particle volume fraction is denoted by φ.

and the improved nanofluid properties play an important role. At high Rayleigh number values convection dominates and improved thermal properties of nanofluids contribute at an lesser extent.

Ra	Air	Water	Water+Cu		Water+Al_2O_3		Water+TiO_2	
			$\varphi = 0.1$	$\varphi = 0.2$	$\varphi = 0.1$	$\varphi = 0.2$	$\varphi = 0.1$	$\varphi = 0.2$
				$d = 0.4L$				
10^3	3.781	3.781	5.030	6.591	4.974	6.451	4.788	5.997
10^4	4.233	4.251	5.232	6.667	5.153	6.511	4.974	6.060
10^5	8.331	8.542	9.434	10.05	9.157	9.435	8.926	8.983
				$d = 0.5L$				
10^3	3.985	3.982	5.296	6.941	5.237	6.793	5.042	6.313
10^4	4.542	4.538	5.571	7.051	5.481	6.877	5.294	6.403
10^5	7.597	8.336	9.255	10.21	9.001	9.673	8.762	9.162

Table 6. Nusselt number values for natural convection of nanofluids in a hotstrip. The values were obtained by integrating over the whole hotstrip.

5. Conclusions

We presented a method for solving coupled laminar viscous flow and heat transfer problems. The algorithm solves the velocity-vorticity formulation of Navier-Stokes equations. The boundary vorticity values are obtained by the single domain BEM solution of the kinematics equation, accelerated by kernel expansion based approximation technique. The solution of the vorticity equation for domain vorticity values, the energy equation for domain temperature values and the kinematics equation for domain velocity values are obtained by subdomain BEM.

The method was used to simulate natural convection phenomena in inclined parallelepiped shaped cavity as well as around a hotstrip. Working fluids were pure air, pure water and water based nanofluids: Cu, Al_2O_3 and TiO_2. The proposed numerical scheme was validated by comparing Nusselt number values with benchmark solutions.

By studying the temperature field in the differentially heated enclosure we observed, that in the central part the temperature field is stratified. The layers of constant temperature are set perpendicularly to the gravity direction regardless of the inclination angle as long as the hot wall lies above the cold wall. The velocity flow fields show that the flow is predominantly moving in a single vortex, up along the hot wall and down along the cold wall. The 3D nature of the flow may be observed in the corners of the enclosures. Comparing the cubic and $H/L = 2$ cavities we established that the Nusselt number values are higher in the case of $H/L = 2$ enclosure.

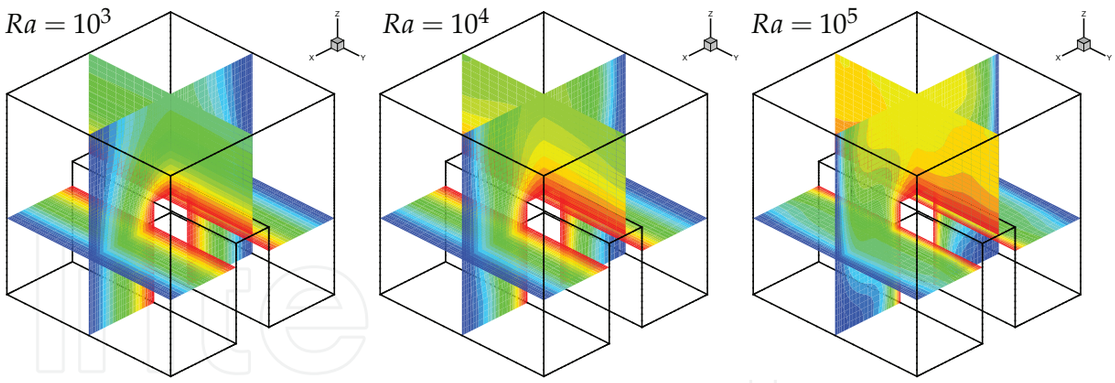

Fig. 7. Temperature contours for natural convection of air around a hotstrip; $d = 0.4L$. Contour values are -0.45(0.05)0.45.

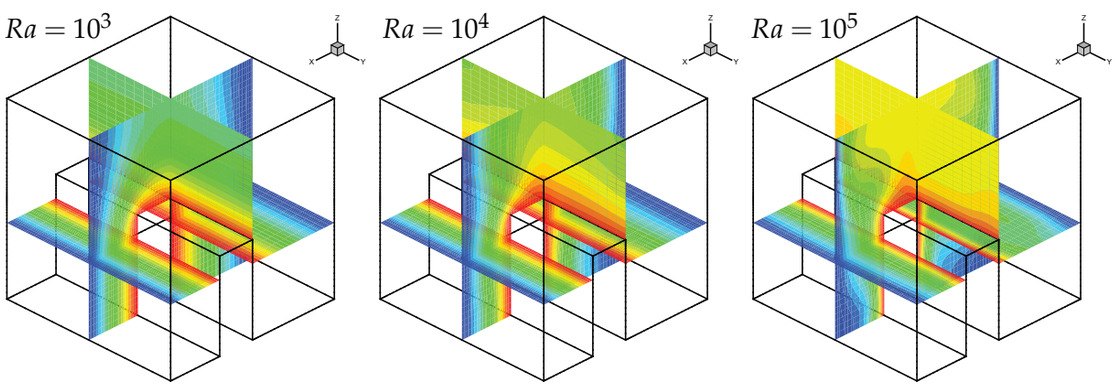

Fig. 8. Temperature contours for natural convection of air around a hotstrip; $d = 0.5L$. Contour values are -0.45(0.05)0.45.

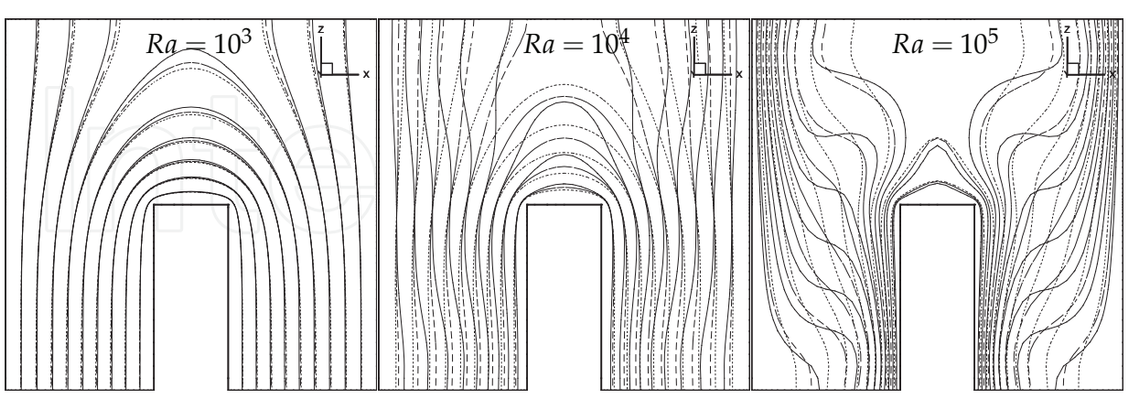

Fig. 9. Temperature contours on the central $y = 0.5H$ plane for natural convection around a hotstrip. Contour values are -0.4(0.1)0.4; Solid line denotes pure water, dashed line Al_2O_3 nanofluid with solid volume fraction $\varphi = 0.1$ and dotted line Al_2O_3 nanofluid with solid volume fraction $\varphi = 0.2$.

A hotstrip in a cavity produces two vortices, one on each side. For $Ra \leq 10^5$ the flow field is symmetric in the case of central placement of the hotstrip. Symmetry is lost when hotstrip is place off-centre. Most of the heat is transferred from the sides of the hotstrip and only a small part from the top wall.
Introduction of nanofluids leads to enhanced heat transfer in all cases. The enhancement is largest when conduction is the dominant heat transfer mechanism, since in this case the increased heat conductivity of the nanofluid is important. On the other hand, in convection dominated flows heat transfer enhancement is smaller. All considered nanofluids enhance heat transfer for approximately the same order of magnitude, *Cu* nanofluid yielding the highest values. Heat transfer enhancement grows with increasing solid particle volume fraction in the nanofluid. The differences between temperature fields when using different nanofluids with the same solid nanoparticle volume fraction are small.
In future the proposed method for simulating fluid flow and heat transfer will be expanded for simulation of unsteady phenomena and turbulence.

6. References

Abu-Nada, E. (2008). Application of nanofluids for heat transfer enhancement of separated flows encountered in a backward facing step, *Int. J. Heat Fluid Fl.* 29: 242–249.

Abu-Nada, E. & Oztop, H. F. (2009). Effects of inclination angle on natural convection in enclosures filled with cuwater nanofluid, *Int. J. Heat Fluid Fl.* 30: 669–678.

Akbarinia, A. & Behzadmehr, A. (2007). Numerical study of laminar mixed convection of a nanofluid in horizontal curved tubes, *Applied Thermal Engineering* 27: 1327–1337.

Bebendorf, M. (2000). Approximation of boundary element matrices, *Numer. Math* 86: 565–589.

Bebendorf, M. & Rjasanow, S. (2003). Adaptive low rank approximation of collocation matrices, *Computing* 70: 1–24.

Brinkman, H. C. (1952). The viscosity of concentrated suspensions and solutions, *J. Chem. Phys.* 20: 571–581.

Bui, T. T., Ong, E. T., Khoo, B. C., Klaseboer, E. & Hung, K. C. (2006). A fast algorithm for modeling multiple bubbles dynamics, *J. Comput. Phys.* 216: 430–453.

Choi, S. U. S. (1995). Enhancing thermal conductivity of fluids with nanoparticles, *Develop. Appl. Non Newtonian Flows* 66: 99–106.

Corvaro, F. & Paroncini, M. (2008). A numerical and experimental analysis on the natural convective heat transfer of a small heating strip located on the floor of a square cavity, *Applied Thermal Engineering* 28: 25–35.

Corvaro, F. & Paroncini, M. (2009). An experimental study of natural convection in a differentially heated cavity through a 2D-PIV system, *Int. J. Heat Mass Transfer* 52: 355–365.

Daube, O. (1992). Resolution of the 2D Navier-Stokes equations in velocity-vorticity form by means of an influence matrix technique, *J. Comput. Phys.* 103: 402–414.

Davies, G. D. V. (1983). Natural convection of air in a square cavity: a bench mark numerical solution, *Int. J. Numer. Meth. Fl.* 3: 249–264.

Eppler, K. & Harbrecht, H. (2005). Fast wavelet BEM for 3D electromagnetic shaping, *Applied Numerical Mathematics* 54: 537–554.

Fata, S. N. (2010). Treatment of domain integrals in boundary element methods, *Applied Numer. Math* .

Gao, X. W. & Davies, T. G. (2000). 3D multi-region BEM with corners and edges, *Int. J. Solids Struct.* 37: 1549–1560.

Greengard, L. & Rokhlin, V. (1987). A fast algorithm for particle simulations, *J. Comput. Phys.* 73: 325–348.

Gumerov, N. A. & Duraiswami, R. (2006). Fast multipole method for the biharmonic equation in three dimensions, *J. Comput. Phys.* 215: 363–383.

Gümgüm, S. & Tezer-Sezgin, M. (2010). DRBEM Solution of Natural Convection Flow of Nanofluids with a Heat Source, *Eng. Anal. Bound. Elem.* 34: 727–737.

Hackbusch, W. (1999). A sparse matrix arithmetic based on $\mathcal{H}$-matrices. Part I: Introduction to $\mathcal{H}$-matrices, *Computing* 62: 89–108.

Hackbusch, W. & Nowak, Z. P. (1989). On the fast multiplication in the boundary element method by panel clustering, *Numerische Mathematik* 54: 463–491.

Ho, C., Chen, M. & Li, Z. (2008). Numerical simulation of natural convection of nanofluid in a square enclosure: Effects due to uncertainties of viscosity and thermal conductivity, *Int. J. Heat Mass Transfer* 51: 4506–4516.

Hsieh, K. J. & Lien, F. S. (2004). Numerical modelling of buoyancy-driven turbulent flows in enclosures, *Int. J. Heat Fluid Fl.* 25(4): 659–670.

Hwang, K. S., Lee, J.-H. & Jang, S. P. (2007). Buoyancy-driven heat transfer of water-based Al_2O_3 nanofluids in a rectangular cavity, *Int. J. Heat Mass Transfer* 50: 4003–4010.

Ingber, M. S. (2003). A vorticity method for the solution of natural convection flows in enclosures, *Int. J. Num. Meth. Heat & Fluid Fl.* 13: 655–671.

Jumarhon, B., Amini, S. & Chen, K. (1997). On the boundary element dual reciprocity method, *Eng. Anal. Bound. Elem.* 20: 205–211.

Khanafer, K., Vafai, K. & Lightstone, M. (2003). Buoyancy-driven heat transfer enhancement in a two-dimensional enclosure utilizing nanofluids, *Int. J. Heat Mass Transfer* 46: 3639–3653.

Liu, C. H. (2001). Numerical solution of three-dimensional Navier Stokes equations by a velocity - vorticity method, *Int. J. Numer. Meth. Fl.* 35: 533–557.

Lo, D., Young, D., Murugesan, K., Tsai, C. & Gou, M. (2007). Velocity-vorticity formulation for 3D natural convection in an inclined cavity by DQ method, *Int. J. Heat Mass Transfer* 50: 479–491.

Mirmasoumi, S. & Behzadmehr, A. (2008). Effect of nanoparticles mean diameter on mixed convection heat transfer of a nanofluid in a horizontal tube, *Int. J. Heat Fluid Fl.* 29: 557–566.

Ögüt, E. B. (2009). Natural convection of water-based nanofluids in an inclined enclosure with a heat source, *International Journal of Thermal Sciences* 48: 2063–2073.

Ong, E. & Lim, K. (2005). Three-dimensional singular boundary element method for corner and edge singularities in potential problems, *Eng. Anal. Bound. Elem.* 29: 175–189.

Oztop, H. F. & Abu-Nada, E. (2008). Natural convection of water-based nanofluids in an inclined enclosure with a heat source, *Int. J. Heat Fluid Flow* 29: 1326–1336.

Paige, C. C. & Saunders, M. A. (1982). LSQR: An algorithm for sparse linear equations and sparse least squares, *ACM Transactions on Mathematical Software* 8: 43–71.

Partridge, P., Brebbia, C. & Wrobel, L. (1992). *The dual reciprocity boundary element method*, Computational Mechanics Publications Southampton, U.K. ; Boston : Computational Mechanics Publications ; London ; New York.

Peng, S. H. & Davidson, L. (2001). Large eddy simulation for turbulent buoyant flow in a confined cavity, *Int. J. Heat Fluid Fl.* 22: 323–331.

Popov, V., Power, H. & Škerget, L. (eds) (2007). *Domain Decomposition Techniques for Boundary Elements: Applications to fluid flow*, WIT press.

Popov, V., Power, H. & Walker, S. P. (2003). Numerical comparison between two possible multipole alternatives for the BEM solution of 3D elasticity problems based upon Taylor series expansions, *Eng. Anal. Bound. Elem.* 27: 521–531.

Press, W. H., Teukolsky, S. A., Vetterling, W. T. & Flannery, B. P. (1997). *Numerical Recipes - The Art of Scientific computing, Second Edition*, Cambridge University Press.

Ramšak, M. & Škerget, L. (2007). 3D multidomain BEM for solving the Laplace equation, *Eng. Anal. Bound. Elem.* 31: 528–538.

Ravnik, J. & Škerget, L. (2009). Natural convection around a 3D hotstrip simulated by BEM, *Mesh Reduction Methods BEM/MRM XXXI*, pp. 343–352.

Ravnik, J., Škerget, L. & Hriberšek, M. (2004). The wavelet transform for BEM computational fluid dynamics, *Eng. Anal. Bound. Elem.* 28: 1303–1314.

Ravnik, J., Škerget, L. & Hriberšek, M. (2006). 2D velocity vorticity based LES for the solution of natural convection in a differentially heated enclosure by wavelet transform based BEM and FEM, *Eng. Anal. Bound. Elem.* 30: 671–686.

Ravnik, J., Škerget, L. & Hriberšek, M. (2010). Analysis of three-dimensional natural convection of nanofluids by BEM, *Eng. Anal. Bound. Elem.* 34: 1018–1030.

Ravnik, J., Škerget, L. & Žunič, Z. (2008). Velocity-vorticity formulation for 3D natural convection in an inclined enclosure by BEM, *Int. J. Heat Mass Transfer* 51: 4517–4527.

Ravnik, J., Škerget, L. & Žunič, Z. (2009a). Combined single domain and subdomain BEM for 3D laminar viscous flow, *Eng. Anal. Bound. Elem.* 33: 420–424.

Ravnik, J., Škerget, L. & Žunič, Z. (2009b). Comparison between wavelet and fast multipole data sparse approximations for Poisson and kinematics boundary – domain integral equations, *Comput. Meth. Appl. Mech. Engrg.* 198: 1473–1485.

Ravnik, J., Škerget, L. & Žunič, Z. (2009c). Fast single domain–subdomain BEM algorithm for 3D incompressible fluid flow and heat transfer, *Int. J. Numer. Meth. Engng.* 77: 1627–1645.

Sellountos, E. & Sequeira, A. (2008). A Hybrid Multi-Region BEM / LBIE-RBF Velocity-Vorticity Scheme for the Two-Dimensional Navier-Stokes Equations, *CMES: Computer Methods in Engineering and Sciences* 23: 127–147.

Shukla, R. K. & Dhir, V. K. (2005). Numerical study of the effective thermal conductivity of nanofluids, *ASME Summer Heat Transfer Conference*.

Škerget, L., Hriberšek, M. & Žunič, Z. (2003). Natural convection flows in complex cavities by BEM, *Int. J. Num. Meth. Heat & Fluid Fl.* 13: 720–735.

Škerget, L. & Samec, N. (2005). BEM for the two-dimensional plane compressible fluid dynamics, *Eng. Anal. Bound. Elem.* 29: 41–57.

Tiwari, R. K. & Das, M. K. (2007). Heat transfer augmentation in a two-sided lid-driven differentially heated square cavity utilizing nanofluids, *Int. J. Heat Mass Transfer* 50: 2002–2018.

Torii, S. (2010). Turbulent Heat Transfer Behavior of Nanofluid in a Circular Tube Heated under Constant Heat Flux, *Advances in Mechanical Engineering* 2010: Article ID 917612, 7 pages.

Tric, E., Labrosse, G. & Betrouni, M. (2000). A first incursion into the 3D structure of natural convection of air in a differentially heated cubic cavity, from accurate numerical simulations, *Int. J. Heat Mass Transfer* 43: 4034–4056.

Vierendeels, J., Merci, B. & Dick, E. (2001). Numerical study of the natural convection heat transfer with large temperature differences, *Int. J. Num. Meth. Heat & Fluid Fl.* 11: 329–341.

Vierendeels, J., Merci, B. & Dick, E. (2004). A multigrid method for natural convective heat transfer with large temperature differences, *Int. J. Comput. Appl. Math.* 168: 509–517.

Wang, X.-Q. & Mujumdar, A. S. (2007). Heat transfer characteristics of nanofluids: a review, *International Journal of Thermal Sciences* 46: 1–19.

Weisman, C., Calsyn, L., Dubois, C. & Quéré, P. L. (2001). Sur la nature de la transition a l'instationare d'un ecoulement de convection naturelle en cavite differentiellement chauffee a grands ecarts de temperature, *Comptes rendus de l'academie des sciences Serie II b, Mecanique* pp. 343–350.

Wong, K. L. & Baker, A. J. (2002). A 3D incompressible Navier-Stokes velocity-vorticity weak form finite element algorithm, *Int. J. Num. Meth. Fluids* 38: 99–123.

Wrobel, L. C. (2002). *The Boundary Element Method*, John Willey & Sons, LTD.

Xin, S. & Quéré, P. L. (1995). Direct numerical simulations of two-dimensional chaotic natural convection in a differentially heated cavity of aspect ratio 4, *J. Fluid Mech.* 304: 87–118.

Yang, Y., Zhang, Z. G., Grulke, E. A., Anderson, W. B. & Wu, G. (2005). Heat transfer properties of nanoparticle-in-fluid dispersions (nanofluids) in laminar flow, *Int. J. Heat Mass Transfer* 48: 1107–1116.

Žunič, Z., Hriberšek, M., Škerget, L. & Ravnik, J. (2007). 3-D boundary element-finite element method for velocity-vorticity formulation of the Navier-Stokes equations, *Eng. Anal. Bound. Elem.* 31: 259–266.

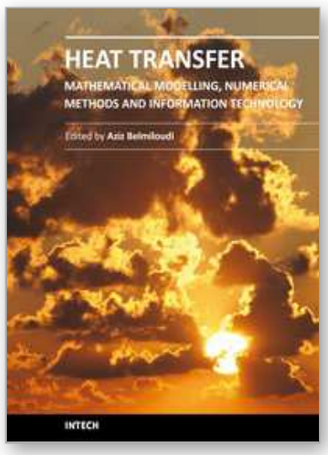

Heat Transfer - Mathematical Modelling, Numerical Methods and Information Technology

Edited by Prof. Aziz Belmiloudi

ISBN 978-953-307-550-1
Hard cover, 642 pages
Publisher InTech
Published online 14, February, 2011
Published in print edition February, 2011

Over the past few decades there has been a prolific increase in research and development in area of heat transfer, heat exchangers and their associated technologies. This book is a collection of current research in the above mentioned areas and describes modelling, numerical methods, simulation and information technology with modern ideas and methods to analyse and enhance heat transfer for single and multiphase systems. The topics considered include various basic concepts of heat transfer, the fundamental modes of heat transfer (namely conduction, convection and radiation), thermophysical properties, computational methodologies, control, stabilization and optimization problems, condensation, boiling and freezing, with many real-world problems and important modern applications. The book is divided in four sections : "Inverse, Stabilization and Optimization Problems", "Numerical Methods and Calculations", "Heat Transfer in Mini/Micro Systems", "Energy Transfer and Solid Materials", and each section discusses various issues, methods and applications in accordance with the subjects. The combination of fundamental approach with many important practical applications of current interest will make this book of interest to researchers, scientists, engineers and graduate students in many disciplines, who make use of mathematical modelling, inverse problems, implementation of recently developed numerical methods in this multidisciplinary field as well as to experimental and theoretical researchers in the field of heat and mass transfer.

INTECH
open science | open minds

InTech Europe
University Campus STeP Ri
Slavka Krautzeka 83/A
51000 Rijeka, Croatia
Phone: +385 (51) 770 447

InTech China
Unit 405, Office Block, Hotel Equatorial Shanghai
No.65, Yan An Road (West), Shanghai, 200040, China
中国上海市延安西路65号上海国际贵都大饭店办公楼405单元
Phone: +86-21-62489820

Fax: +385 (51) 686 166
www.intechopen.com

Fax: +86-21-62489821

IntechOpen